Towards the controlled release of metal nanoparticles from biomaterials: physico-chemical, morphological and bioactivity features of Cu-containing sol gel glasses

Aina Valentina, Cerrato Giuseppina, Martra Gianmario

[1] Department of Chemistry, University of Torino, Via P. Giuria 7, 10125 Torino, Italy; Centre of Excellence NIS (Nanostructured Interfaces and Surfaces); INSTM (Italian National Consortium for Materials Science and Technology), UdR University of Torino.

Malavasi Gianluca,* Lusvardi Gigliola, Menabue Ledi.

[2] Department of Chemical and Geological Science, University of Modena and Reggio Emilia, Via Campi 183, 41125 Modena, Italy.

Corresponding Author:

* to whom correspondence should be addressed:

Department of Chemical and Geological Science, University of Modena and Reggio Emilia, Via Campi 183, 41125 Modena, Italy, E-mail address: gmalavasi@unimo.it

Tel +390592055041; Fax +39059373543

Abstract

Two Cu-containing bioactive glasses were prepared and characterized in order to obtain a detailed description of chemical, morphological and bioactivity proprieties of potential Cu releasing systems. The characterization has demonstrated that by varying the synthesis procedure is possible to obtain two systems with Cu species in two different oxidation states and aggregation: *i)* SGCu(ox) – oxidated Cu – (Cu oxidation state +2) homogeneously dispersed in the glass network matrix and *ii)* SGCu(red) – metallic Cu – (Cu oxidation state 0) containing nano-particles (5-130 ~~120~~ nm range) mainly present on the glass surface. The introduction of Cu maintains the bioactivity of the Cu-containing glasses almost unchanged, inducing a partial delay in the hydroxyapatite/hydroxy-carbonate apatite (HA/HCA) formation on the glass surface with respect to the reference glass (free Cu glass). During the bioactivity test, Cu is released from both Cu-containing glasses, in particular in the case of the SGCu(red) the presence of Cu nanoparticles (CuNPs) of diameter in the range 5-10 nm has been detected in solution.

Keywords: Cu-containing glasses; Cu nanoparticles (CuNPs); Cu ions; physico-chemical characterization; *in-vitro* bioactivity

Introduction

Nowadays, nanotechnology is playing an important role in the field of biomedicine and nanoparticles are widely used in both biomedical and biological applications. [1-3]

Metal nanoparticles, due to their conspicuous physico-chemical properties, have received considerable attention. Particularly Ag [4,5] and Au nanoscaled [1,6-9] particles because of their attractive optical properties have been widely studied. One significant approach is to prepare nanoparticles in the presence of supporting materials like aluminium or titanium oxide, polymers, mesoporous silica and ceramics that can act as novel hosts for the immobilization of metallic nanoparticles. [10-12]

Despite Au and Ag, the usefulness of Cu as an antibacterial agent has been known for a long time: if Cu is deposited on supporting material, the releasing time of Cu can be slowed down for a long time so that Cu-supported materials will be of great potential for antibacterial applications. [13-15]

Especially metal-supported silica materials (such as silica glass and silica thin films) are expected to be good candidates for antibacterial materials due to their fine chemical durability and high antibacterial activity. [16,17] Mesoporous copper-doped silica xerogel with antibacterial properties were synthesized by a sol-gel process and these studies showed that the antibacterial activity was related to size and morphogenesis of the nanoparticles. [18-21]

In particular, the introduction of metal nanoparticles (Au, Ag and Cu NPs) onto the glass surface are very useful, because NPs can directly act as: *(i)* bactericides (Ag, Cu NPs), [21] *(ii)* imaging agents;[22-24] moreover, they can be used to immobilize, via a covalent linkage, an enzyme/protein and/or a drug on the glass surface through the formation of self-assembled monolayers (SAMs), in order to obtain a stable bio-conjugate systems. [7]

In 1991 Li *et. al*. [25] synthesized some bioactive glasses in ternary SiO_2-CaO- P_2O_5 system by sol-gel route and found that hydroxyapatite (HA) is deposited much faster on sol-gel bioactive glasses than on traditional melt derived bioactive glasses. The secret lies in the synthesis procedure, which is performed in aqueous environment and then dried and stabilized at temperature that does not exceed 600°C. In 2001 molecular biology studies performed by Xynos *et. al.* [26,27] showed that control rate of release of ionic dissolution products of bioactive glasses plays major role in their bioactive behaviour. Thereafter bioactive glasses were being fabricated in order to increase their stimulating effect on osteogenesis, angiogenesis and the promotion of antibacterial properties. [28] This could be achieved by doping different trace elements of biological significance in the glass network. Doping corresponds to the deliberate introduction of elements (atoms, ions, molecules) in a given material usually to improve its properties. Doping elements are found at low concentration compared to the main elements of the materials typically ranging from few ppm to few percent. Once again, sol-gel process appears to be an ideal route for the controlled doping of materials. The process provides

material with good chemical homogeneity, yielding material with homogenous properties. Another advantage is its high versatility which allows easy variation of the nature of the doping species and of their concentration. [29]

Our purpose is to dope bioactive glass with copper and to find the better condition for CuNPs formation into the glass matrix: this allow us to prepare a biomaterial able to joint the bioactivity with the possibility of a controlled release of Cu nanoparticles with antibacterial properties in the implantation sites. In this paper, the study of Cu-bioactive glasses nanocomposites has been carried out on two Cu-containing glasses in comparison with the reference sol-gel ternary glass ($15CaO{\cdot}5P_2O_5{\cdot}80SiO_2$). The evolution of copper nanoparticles and aggregates as a function of the thermal treatment that induces the nucleation of Cu nanoparticles into aggregates of different size has been evaluated. A thorough physico-chemical characterization has been also carried out in order to obtain a detailed description of these new types of bioactive glasses (containing Cu-nanoparticles). Moreover, i*n-vitro* glasses bioactivity tests were performed in order to evaluate ions (Ca, P, Si) and Cu nanoparticles release as a function of reaction time in simulated body fluid (SBF) and the subsequent evolution of glasses structure during the reaction.

Materials and Methods

Materials

Glasses synthesis

Two glass systems, with theoretical molar composition $15CaO \cdot 5P_2O_5 \cdot 80SiO_2 \cdot xCuO$ (with x=0 and 1; the copper amount is conventionally indicated in the oxidic form CuO), were synthesized using a sol-gel route. The gels were then treated at 873K for 2 hours in flowing N_2 atmosphere (0.3L/min) to stabilize the glass system (elimination of solvents and reagents residues) as reported in previous paper.[30] The samples are referred to in the following as SG and SGCu(ox), respectively.

Another synthesis route (impregnation) was carried out on the SG glass in order to obtain the reduction of Cu^{2+} ions to Cu nanoparticles. This procedure was optimized in a previous paper: [30] briefly, 2 g of SG were soaked for 1 h in 14 ml of $Cu(NO_3)_2 \cdot 3H_2O$ 0.28 M; the obtained blue gel was aged at 333K and treated at 973K in N_2/H_2 atmosphere for 2 hours and this sample is referred to as SGCu(red). After thermal treatments at 873K, Cu-containing powders (SGCu(ox)) were blue coloured, whereas after calcination at 973K in N_2/H_2 (0.3L/min) atmosphere (SGCu(red)) were brown-red coloured. These calcined powders were ground in an agate mortar and sieved in order to isolate the fraction of particles with ϕ <50μm.

The glass powders were used to prepare a soluble glass (ratio between glass powder and $LiBO_2$ = 0.1 g : 0.9 g) and after dissolution the solutions were analysed by ICP in order to determine the experimental concentration of the samples. In **Table 1** the glasses experimental compositions, in molar %, are reported. The amount of Cu was conventionally expressed as CuO molar %.

Methods

Morphological characterization

Specific surface area and porosity measurements (N_2 adsorption at 77K)

Specific surface area (SSA) and porosity were evaluated by adsorption of an inert gas (N_2) at the temperature of liquid nitrogen (77K) using a Micromeritics ASAP 2020 porosimeter. For specific surface area determination data were analyzed with the BET model (Brunauer, Emmet and Teller). [31] BJH model (Barrett-Joyner-Halenda) [32] was used to analyze mesopores, and 't-plot' (statistical thickness method) [33] was employed to evaluate the presence of micropores.

The accuracy of BET model for SSA determination is known to be *per se* relatively low (~ 5%), whereas both instrumental accuracy and reproducibility of data obtained with modern automatic gas-volumetric instrumentation are quite high. For a review on those methods, see Gregg and Sing. [34]

Before the measurements, all the samples were out-gassed at room temperature (RT) for 12 h under vacuum (Final pressure $1{,}33 \cdot 10^{-2}$ Pa).

Transmission electron microscopy (TEM)

High-Resolution Trasmission Electon Microscopy (HR-TEM) images were obtained with a JEOL 3010-UHR (acceleration potential of 300 kV, LaB_6 filament). The microscope was equipped with an Oxford INCA X-ray energy dispersive spectrometer (X-EDS) with a Pentafet Si(Li) detector. Samples were "dry" dispersed on lacy carbon Cu grids.

Surface characterization

Infrared Spectroscopy (IR)

Carbon Oxide (CO) adsorption at 77K: Infrared Spectroscopy (IR) can be used for the identification and characterization of surface species and also to study the adsorption/desorption features of suitable probe molecules. [35-36]

Experiments of CO adsorption at 77K: The samples were inserted in a home-made glass and metal cell, described elsewhere [37,38] that allows all thermal treatments, gas-solid adsorptions and spectral recordings at 77 K to be carried out in a strictly *in situ* configuration. All IR spectra were recorded using a FTIR (Bruker IFS 28 spectrophotometer, equipped with both MCT (mercury-cadmium-teluride) and DTGS (deuterated triglycine sulphate) detectors) in the 4000-400 cm^{-1} spectral range. Before CO adsorption, samples were activated at 673K in presence of O_2 for 1h (in order to remove carbonates species), then the samples were re-hydrated with purified H_2O at RT and then outgassed at 423K for 1h. IR spectra were normalized to both BET surface area and sample weight (to the total surface area exposed).

The roto-vibrational contribution of the gaseous CO phase was subtracted from the CO adsorption spectra. [39]

KBr pellets: KBr pellets of samples before and after SBF contact were prepared by mixing under controlled conditions (glovebox) 1 mg of either starting powder or filtered reacted powder with 50 mg of specpure KBr. Transmission spectra of KBr pellets were normally recorded using a DTGS detector in order to inspect also the low-ν region of the 4000-400 cm^{-1} spectral range and performing 128 scans for each measurement.

Bioactivity tests

There is a generally-established relationship between the ability of a given material to form bonds with living tissues and its ability to grow an apatite-like layer when soaked in fluids mimicking human plasma, and for this reason in vitro assays are common and widely employed tools in the bioactivity study of new candidate implant materials. In this study, in order to monitor bioactivity, we used the simulated body fluid (SBF) proposed by Kokubo *et. al.* [40] (an acellular aqueous solution with an inorganic ion composition almost equal to human plasma).

The bioactivity response of the materials was evaluated in terms of the formation of a HA/HCA layer on the surface of 250 mg of powdery samples after being soaked in 50 mL of SBF at different

times (1, 4, 7 and 14 days) at 310K. The materials resulting coated by a HA/HCA layer were considered bioactive, whereas if the glass surface remained unchanged after the SBF treatment, the materials have to be considered non bioactive. Furthermore, in vitro studies allowed us to compare for different samples the relative kinetics of the bioactive response: the shorter the time required for the HA/HCA layer formation, the higher the bioactivity of the material.

The HA and/or HCA formation has been monitored by X-ray powders diffraction (XRPD) and Fourier Transformed Infrared (FTIR) spectroscopy.

X-ray powders diffraction (XRPD) diffraction

XRPD (X-ray powders diffraction) patterns were recorded on a PANalytical X'Pert Pro Brag-Brentano diffractometer, using Ni-filtered Cu Kα radiation (λ = 1.54060 Å) with X'Celerator detector. The patterns were taken over the diffraction angle 2θ range = 10-50° and with a time step of 50 s and a step size of 0.03°.

SBF (simulated body fluid) solution analysis

In view of the ability of these materials to release Cu, the powders, soaked in SBF for different times (1, 4, 7 and 14 days) were filtered with a Wathman membrane filter, pore size 0.45 μm, diameter = 50mm and then the solutions were analyzed by means of ICP (Inductively Coupled Plasma, Perkin Elmer Optima 4200 DV, USA) for determining Si, Ca, P and Cu content at each above mentioned time. In order to ensure the complete solubilization of the eventually released CuNPs from the SGCu(red) glass, 5 ml of HNO_3 conc. were added to SBF solutions.

Results and Discussion

Synthesis and the preliminary characterization of these glasses were reported in previous paper. [30] It is possible to summarize that XRD patterns showed that the SG and SGCu(ox) samples were completely amorphous, whereas SGCu(red) glass showed the diffraction peaks typical of metallic Cu. Moreover, the presence of Cu metallic particles in the SGCu(red) glass has been confirmed by scanning electron microscopy (SEM-EDX) images: these data showed, in the glass matrix, the presence of aggregates in the range 150-400 nm mainly constituted by Cu. Moreover, by UV-Vis spectra the sample SGCu(red) showed a plasmonic band typical of CuNPs at about 580 nm, but this feature does not exclude the presence of Cu^{2+} species in the glass. In order to clarify the morphology of metal NPs/glass composite and the copper oxidation state in both the SGCu(red) and SGCu(ox) samples, a more detailed characterization study of the synthesized samples has been reported joined with the reactivity in simulated biological fluids.

Specific surface area (SSA) and porosity data are reported in **Table 2**. These data lead some interesting information regarding the effects of *i)* the addition of Cu in the glass composition and *ii)* the thermal treatments on the nanostructure (Cu nanoparticles aggregation).

First of all, the SSA of the reference SG sample, used in the present work, is higher with respect to SSA of SG of our previous works [6,41-42] (360 vs 165 m^2/g) . This is due to the post-synthesis thermal treatment carried out, in the present case, in N_2 atmosphere that allows the better removal of compounds used during the synthesis procedure. On the contrary, in our previous works [6,41-42] the post-synthesis thermal treatments have been performed under static conditions with a reduced efficacy of the removal of compounds.

The SSA of the SG exhibits high surface area (361 m^2/g) whereas the presence of CuO in the glasses composition seems to cause a decrease of SSA 298 and 137 m^2/g in the Cu-glass treated at 873K in N_2 (SGCu(ox)) and in the Cu-glass treated at 973K in N_2/H_2 (SGCu(red)), respectively. Concerning the porosity, the plain SG glass possesses both micropores and mesopores with a mesopores average pore width of around 20 Å.

The impregnation process and the following thermal treatment carried out in reduced atmosphere at 973K causes a significant decrease of mesoporosity and an increase of the microporosity. The glass sintering is likely to start~~s~~ at 973K: there is a condensation of the surface particles with the formation of Cu surface aggregates (**see TEM images, Figure 1c**). Indeed, the increase of microporosity is due to the micropores present inside the Cu aggregates. On the contrary, the decrease of mesopores area with respect to SG and SGCu(ox) is due mainly to the glass sintering process.

Concerning the SGCu(ox) glass, the introduction of Cu in the glass composition causes a decrease of the microporosity with respect to the plain SG glass (23 vs 43 m^2/g), whereas the mesopores area

(109 vs 140 m^2/g) and also the average pores width increase (26 vs 21 Å). In this glass, Cu species (as Cu^{2+}) is homogeneously distributed in the glass matrix (**see EDS image, Figure 1B**), no aggregates are formed and its morphology is quite similar to that of the SG parent glass.

In particular, TEM images and EDS maps obtained for the three glasses are reported in **Figure 1**. A typical TEM micrograph of SG glass is reported in **Figure 1A** as a reference**.** This material appears to be quite porous, in good agreement with the indication coming from N_2 adsorption data: moreover, as reported in the EDS composition maps, Ca, P and Si species are homogeneously distributed in the glass particles.

By the inspection of the TEM images obtained for the the SGCu(ox) **(Figure 1B)** Cu appears highly and homogeneously dispersed into/onto the silica matrix. As for the morphology of the amorphous phase present in the SGCu(ox), it can be observed that the presence of Cu induces almost no alteration in the typical features ascribable to the plain glass and, as suggested by EDS analyses, all the elements (included Cu) are homogeneously distributed in the glass matrix.

A TEM image of SGCu(red) glass is reported in **Figure 1C**. This material, as indicated also by N_2 adsorption data, appears quite porous and the presence of sub-micrometric Cu particles is now evident: these are characterized by dimensions in the 5-130 nm range in diameter and often gathered in aggregates. This result give a more datailed description with respect the morphological analysis performed by SEM in the past work.[30] In fact the conclusion obtained in the above mentioned work showed Cu nanoparticles in the range of 150-400 nm while this study clarified that the particles put in light by SEM analysis were big aggregates constituted to smaller nanoparticles of dimension in the range 5-130 nm. It is likely that both impregnation procedure and thermal treatment at 973 K in N_2/H_2 atmosphere caused the coalescence of the Cu nanoparticles with the formation of surface Cu aggregates and the particle size trend is consistent with what reported previously.[30] In this system the surface segregation of Cu nanoparticles is evident: they are mainly composed of Cu, whereas the glass matrix is made up of Ca, P and Si elements (see EDS maps). TEM analysis allows also to determine almost exactly the size of each individual nanoparticle: this is reported in **Figure 2,** in which the distribution of Cu nanoparticles in the SGCu(red) sample is ascribable.

Figure 3 reports the IR spectra (in the region 2200-2080) relative to the adsorption of CO at 77K on SG **(Section A)**, SGCu(ox) **(Section B)** and SGCu(red) **(Section C)** in contact with different CO amounts. Differential spectra were obtained with respect to the background spectrum of the glass out-gassed at 423K (after a preliminary treatment at 673K and subsequent rehydration with purified distilled water at RT).

The thermal pre-treatment promoted the desorption of water molecules from the glasses' surface, mostly leaving some coordinatively unsaturated species (i.e. *cus* cations) able to interact with CO,

acting as probe molecule. The activation conditions represent a good compromise between number of cationic surface sites accessible by CO and extension of surface modification. In this respect, significant information can be provided by the study of the IR spectra of adsorbed CO, as well-known in the field of surface science applied to heterogeneous catalysts. [43,45] In fact, different ionic and metallic sites can be differentiated on the basis of both frequency and stability of their surface carbonyl species formed after CO adsorption.

By the inspection of **Figure 3A,** which refers to CO adsorbed at 77K on the SG glass, it can be evidenced that, after CO adsorption, it is possible to single out only one carbonyl-like component centred at ~ 2155 cm^{-1}. As far as CO coverage decreases, **(see curve b-e in Figure 3A)** the intensity of the band progressively decreases, indicating that the interaction is almost totally reversible. On the basis of both spectral behaviour and of literature data, [44,45] this band can be attributed to CO molecules in interaction with *cus* Ca^{2+} species, acting as weak Lewis acid sites, as also reported for penta-coordinated Ca^{2+} at the surface of CaO. [45]

In the case of the SGCu(ox) sample **(see Figure 3B)** a more complex situation is observable: the ~ 2155 cm^{-1} band is still present, but, after CO adsorption another component appears at higher frequencies. It is located at ~ 2162 cm^{-1} for high CO pressure, and this band might be a result of CO molecules adsorbed on Cu^{2+} sites, [44] as also observed for other Cu^{2+} containing systems inspected by CO adsorption. [44]

Finally, the spectra relative to SGCu(red) CO adsorption are reported (see **Figure 3C**). In this case, a new spectral component, located at ~ 2137 cm^{-1}, is evident. On the basis of its spectral behaviour and of literature data [44], this band can be ascribable to CO adsorption onto surface Cu metallic sites.

Bioactivity tests

In order to ascertain the possible bioactivity developed by the above mentioned Cu-containing SG glasses, some tests were carried out after different times (1, 4, 7 and 14 days) of reaction in SBF: the solutions have been filtered and the resulting dried powders have been characterized by means of both XRD diffraction and FT-IR spectroscopy, whereas the SBF solutions have been analyzed by ICP.

Powders characterization

Figure 4 reports the XRD patterns of the samples before and after SBF soaking. As previously reported by Shruti *et al.*, [47] a very weak broad peak at 2θ ~32°, tentatively assigned to the (211) HA reflection, was evident in the almost amorphous pattern of SG sample, after 1 day of reaction in SBF. On the contrary, the main peak of HA, centred at 2θ ~31.6° was observed in the XRD patterns of SGCu(ox) only after 4 days of soaking. After 14 days of SBF soaking the XRD patterns of SG and SGCu(ox) glasses exhibited an increase of HA peaks intensity.

SGCu(red) spectra of as synthesised (a.s) sample showed a broad enveloped centered at 22° in 2θ characteristic of a phosphate-silicate based glass and two diffraction peaks corresponding to metallic Cu (111 and 200, JCPDS 04-0836). Concerning SGCu(red) sample as the soaking time increases, XRD patterns exhibited a intensity decrease of the two peaks attributed to metallic Cu, probably due to the release of CuNPs without any evidence of HA/HCA formation.

These data indicate that the presence of Cu in the oxidized form causes only a slight delay in the HA/HCA formation on the glass surface. This delay is most likely due to competition between Cu^{2+} and Ca^{2+} ions in solution for the precipitation of phosphate species. On the contrary, the presence of metallic CuNPs in the glass matrix and the higher thermal treatment temperature seems to inhibit the HA/HCA deposition on the SGCu(red) sample surface.

Figure 5 reports KBr pellet spectra of samples SG, SGCu(ox) and SGCu(red) (**Sections A, B and C,** respectively) as such and after 1, 4, 7 and 14 days of soaking in SBF solution.

Starting from the spectral patterns of the plain SG glass (see **Figure 5, Section A**) it can be noted that, within 4 days of reaction, two main effects become quite evident: *(i)* the appearance of two partly resolved peaks centered at ~611 and ~560 cm^{-1}, typical of HA/HCA formation.[40] This feature is clear evidence for the crystallization of Ca-phosphate on the glass surface, in that the evolution from a single, broad peak at ~580 cm^{-1} (present in the glasses as such) towards a resolved doublet has been long recognized as symptomatic of the formation of a crystalline HA-like phase and thus of potential bioactivity; [40] *(ii)* the disappearance of a broad shoulder band centered at ~940 cm^{-1} and due to the so-called non-bridging oxygen species. [11] The declining intensity of the latter spectral component is very fast as a function of reaction time and monitors the ions release from the glass to the contact solution.

In the case of the sample SGCu(ox) (**Figure 5, Section B**) only after 7 days of reaction (see spectrum d), the two resolved peak typical of HA/HCA crystallization are evident. The presence of Cu^{2+} in the glass composition is likely to be responsible for a slight delay in the HA/HCA crystallization with respect to the reference SG glass.

Concerning the SGCu(red) sample (**Figure 5, Section C**), until 14 days of reaction (see spectrum e) the two resolved peaks centered at ~611 and ~560 cm^{-1}, typical of HA/HCA formation, are never clearly evident. The presence of CuNPs might cause a delay in the HA/HCA formation on the glass surface, and in this respect, FT-IR spectroscopy is more sensitive than XRD to detect even low amount of surface species. For this reason, after 14 days of SBF reaction, in the case of the SGCu(red) sample, it is possible to evidence the presence of a small amount of HA/HCA on the glass surface whereas XRD patterns contain no clear indication for it.

Figure 6 reports the IR spectra (in the region 2200-2080) relative to the adsorption of CO at 77K on SG-873 **(Section A)**, SGCu(ox) **(Section B)** and SGCu(red) **(Section C)** after 14 days of reaction in

SBF in contact with different CO pressures. Differential spectra were obtained with respect to the background spectrum of the glass out-gassed at 423K (after a preliminary treatment at 673K and subsequent reydration with purified distilled water at RT).

As for the SG glass reacted 14 days in SBF, (see **Figure 6, Section A)** after CO adsorption it is possible to observe a component centred at ~ 2152 cm^{-1} due to CO molecules in interaction with *cus* Ca^{2+} species, as already reported for the unreacted powders (vide infra).

Concerning the SGCu(ox) sample reacted 14 days in SBF **(see Figure 6, Section B),** upon CO adsorbtion, almost the same spectral features are observed.

On the contrary, in the case of the SGCu(red) (**Figure 6, Section C)** two components are now evident: apart the 2155 cm^{-1} component, in common with the other spectral pattern previously discussed and ascribed to CO molecules adsorbed onto Ca^{2+} cus sites, [44] there is a second component, located at 2134 cm^{-1}. The latter is ascribable, on the basis of its spectral behaviors and literature data [42] to CO interactions with surface Cu metallic species.

Comparing these spectra with those collected for the unreacted samples it is worth noting that:

- in the case of the plain SG glass, after 14 days of reaction the intensity of the CO component centred at ~2152 cm^{-1} is decreased by times, clear indication of a decreasing of availability of Ca^{2+} species at the glass surface;
- concerning SGCu(ox), the band located at ~ 2162 cm^{-1} (typical of CO molecules adsorbed on Cu^{2+} sites) has disappeared after 14 days of reaction; meaning that Cu^{2+} species have been leached away as a consequence of the soaking in SBF;
- finally, in the case of SGCu(red), there is a general decrease of the intensity on both spectral components after 14 days of reaction. In this case, Cu species (in the form of CuNPs Cu^0) are still present after 14 days of reaction.

Solutions analysis

The concentration trends in SBF solution, during the bioactivity tests, gives some information about samples solubilization/release and new phases formation on the sample surfaces (precipitation). **Table ~~2~~ 3** reports the concentrations (in ppm) of the species present in solution; conventionally the concentrations are reported as Si, Ca, P and Cu although the species present in solution may be other. The concentrations (ppm), measured after different times of glasses reaction in SBF, are reported in **Table 3**, and the data represent the mean value of four different determinations carried out on the same sample solution. In order to test the reproducibility of experiments we had performed two independent replicated experiments for SGCu(ox) sample after 14 days of SBF soaking and the concentration differences between two replicated samples were less than 5%.

In the case of the SG sample, the Ca concentration increased up to 296 ppm after 1 day soaking, and then it decreased whereas for the SGCu(ox) sample the Ca concentration increased (187 ppm) up to

7 days and then it decreased. A different behaviour was detected for the SGCu(red) sample: after 1 day, the Ca concentration increased up to ~140 ppm and it remained quite constant until 14 days of soaking.

Concerning the SG sample, P concentration increases in the first day of reaction and then it decreases whereas in the case of both Cu-containing glasses it increases after 1 day and decreases only after 7 days (SGCu(ox)) and 4 days (SGCu(red)) (see **Table 3**). The largest concentration of P species was detected for SG after 1 day (165 ppm); for longer times, it decreases as previously reported in the case of sol-gel bioactive glasses. [45]

In this case, the attention has been focused to Cu trend in solution. For the SGCu(ox) sample, the Cu concentration detected in SBF solution was lower if compared with that of the SGCu(red) system. This can be due to the lower amount of Cu in the SGCu(ox) glass with respect to SGCu(red) (1.1% vs 2.9% respectively, see **Table 1**). Moreover, it can be assumed that in the SGCu(red) system CuNPs can be easily released because there are located on the glass surface, whereas in the SGCu(ox) glass the Cu^{2+} ions are present in the glass bulk. Although, the Cu concentrations were different, the trend of Cu release was the same for the two Cu-containing systems, in both cases the concentration of Cu increases up to 7 days and then decreased.

All samples exhibit a sudden increase in Si concentration that becomes constant when it reaches the value of ~60-70 ppm.

It is noteworthy that, for the SGCu(red) sample, the concentration of Ca^{2+} in solution after 1 day is the lowest detected. This is most likely due to the lower concentration of CaO in this system (see **Table 1**); moreover, the surface of SGCu(red) samples is mainly covered by CuNPs, thus inhibiting Ca^{2+} ions to be released, as they are located in the inner part of the glass grains. The Ca^{2+} trend in solution may also explain the delay in the formation of HA/HCA layer on the surface of this sample.

Finally, to verify the nature of Cu (either in the form of nanoparticles and/or as ions) released from the SGCu(red) sample a precise amount of the SBF filtered solution, after 7 days of reaction, was spinned, the supernatant removed and the remaining solution was placed on a grid, perfectly dried and then analyzed by TEM microscopy. **Figure 7** reports a TEM image of what was observed: nanoparticles with a diameter in the 5-10 nm range, are evident; EDS analysis (not reported for the sake of brevity) revealed that these nanoparticles are essentially made up of Cu and this evidences the SGCu(red) sample is able to release CuNPs. These results –are in good agreement with the indications coming from both IR spectra and XRD patterns (*vide infra*) confirming the presence of metallic Cu^0.

Conclusion

Two Cu-containing bioactive glasses were successfully synthesized and thoroughly characterized. In the SGCu(ox) sample, Cu species are present in the oxidized state as Cu^{2+} and they are homogeneously distributed in the glass matrix. The bioactivity of this material has been verified in terms of HA/HCA precipitation; if it is compared with the reference SG glass, only a slight~~ly~~ delay in HA/HCA formation was detected despite the low amount (5 ppm) of Cu released in solution.

The CuNPs containing system is mainly characterized by the presence of metallic nanoparticles (in the -130 ~~120~~ nm range) on the glass surface. In this case, the amount of Cu released is very high, as the maximum Cu concentration reached was 65 ppm. The delay in the HA/HCA formation on the SGCu(red) sample is due to the low relase of Ca^{2+} ions, as indicated by ICP data. By the inspection of SGCu(red) morphological features, it is possible to single out that the glass surface is mainly covered by CuNPs and Ca^{2+} species are in the glass bulk.

The presence of Cu metallic nanoparticles confined onto the glass surface (as confirmed by TEM/SEM image) suggests this material to be a good candidate for the interaction with SH groups useful for a covalent immobilization of organic molecules (*i.e.* drugs, enzymes). As briefly reported in the Introduction, copper nanoparticles are used for different medical applications particularly as antibacterial agent but also the presence of Cu surface nanoparticles can be used in binding of biomolecules to the surface of Cu particles has been documented. [20,21,44] For these reasons it is important verify the presence of Cu metal or Cu^{n+} species on the glasses' surface. In this paper a proper control of electronic states of Cu dispersed within the glass matrix has been obtained through the sol-gel synthesis and the different post-synthesis thermal treatments. Moreover, the presence of released Cu, as both Cu^{2+} or NPs, can direcly act as bactericides in the implant site.

Figures

Figure 1. TEM images and EDS compositional maps carried out on SG glass (Section A), SGCu(ox) glass (Section B) and SGCu(red) glass (Section C).

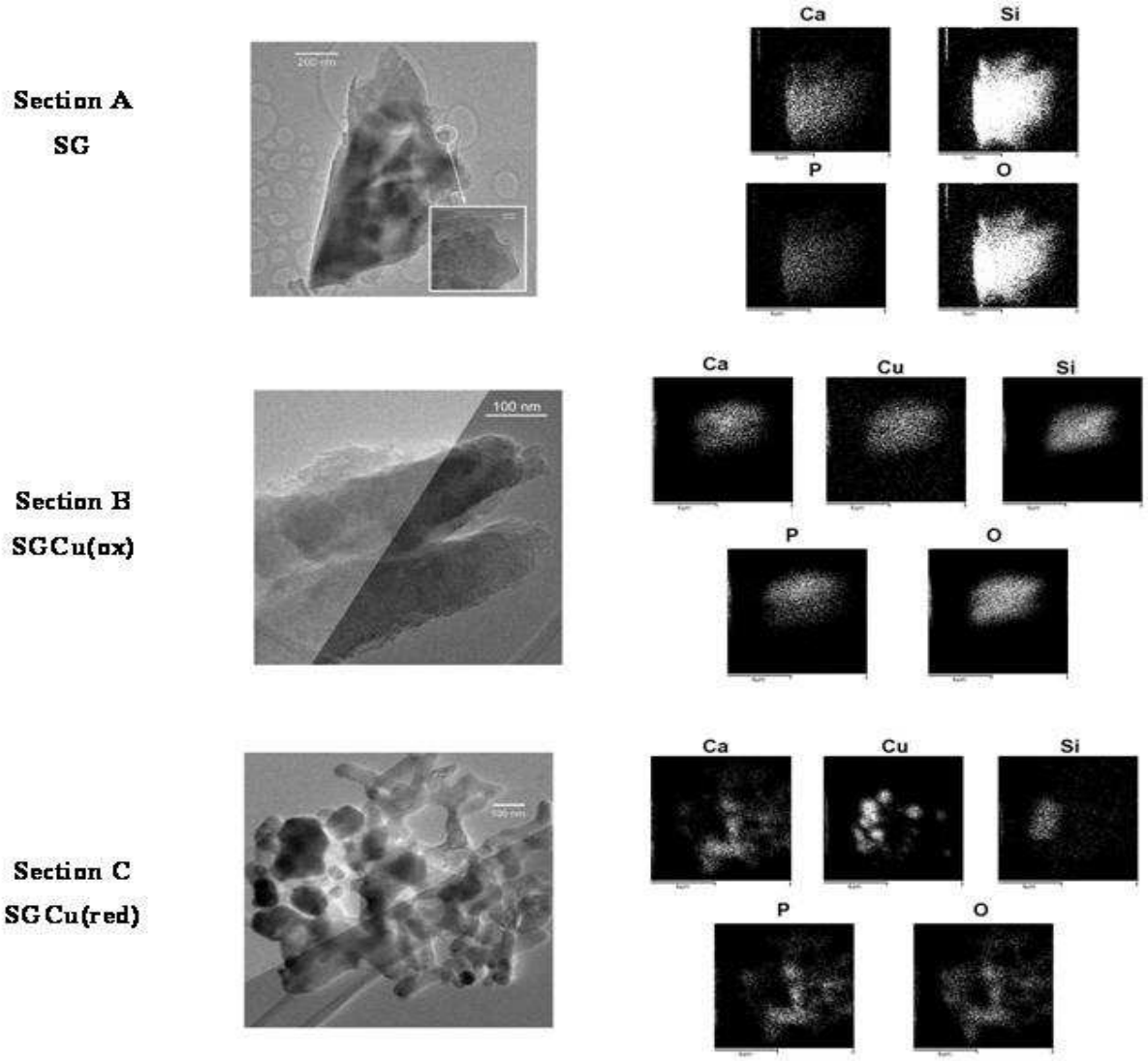

Figure 2. Cu particles size distribution evaluated by TEM images in the SGCu(red) glass.

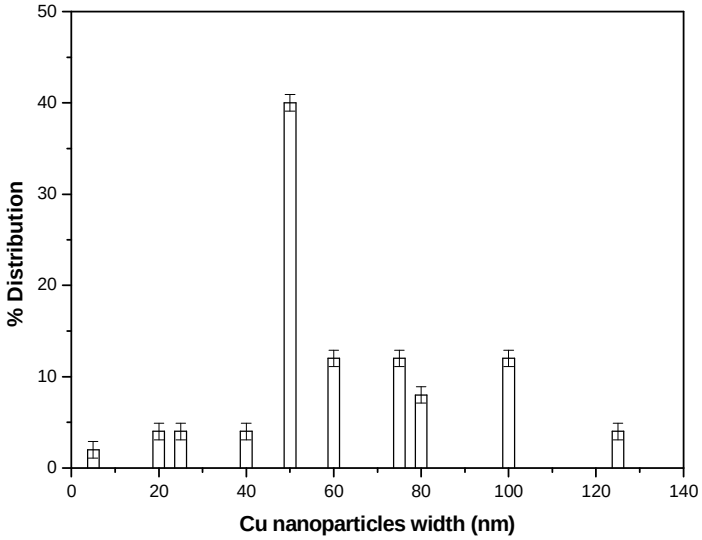

Figure 3. Absorbance differential IR spectra (in the region 2200-2080) relative to the adsorption of CO at 77K on SG (A), SGCu(ox) (B) and SGCu(red) (C) in contact with (a) 50 Torr of CO; (b) 25 Torr of CO; (c) 10 Torr of CO; (d) 5 Torr of CO; (e) 2 Torr of CO. Differential spectra were obtained with respect to the background spectrum of the glass out-gassed at 423K (after a preliminary treatment at 673K and subsequent rehydration with purified distilled water at RT; see text).

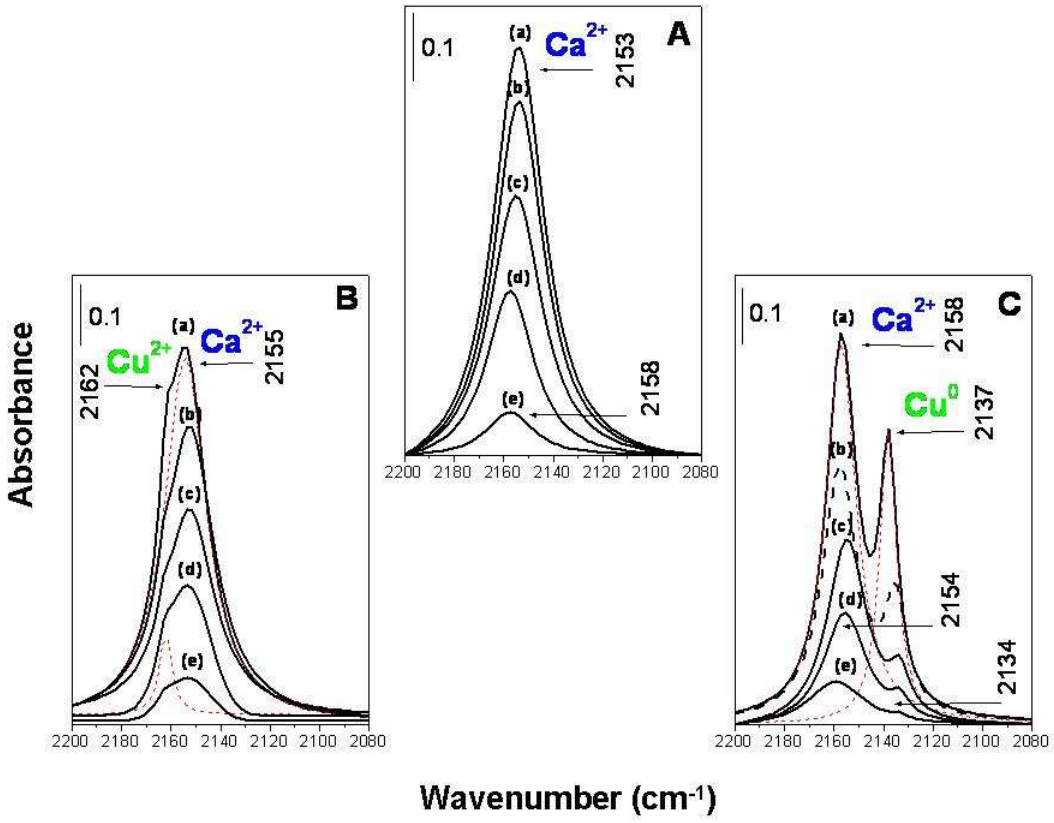

Figure 4. XRD patterns showing the effect of up to 7 days reaction in SBF solution of glasses SG (a), SGCu(ox) (b) and SGCu(red) (c) as such and after soaking in SBF solution.

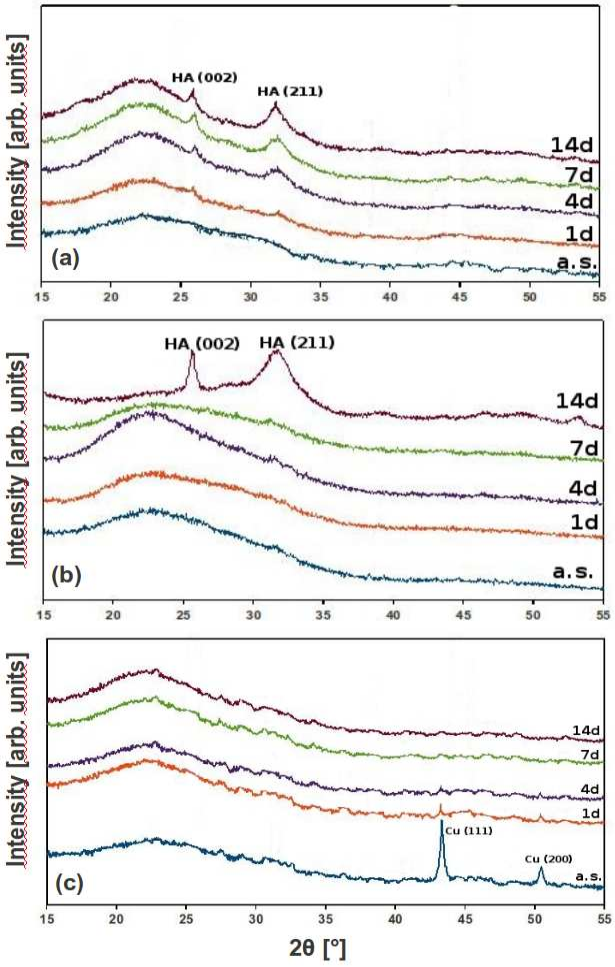

Figure 5. FTIR spectra, in the 1800-400 cm^{-1} range, of KBr-pellet specimens, showing the effect of up to 7 days reaction in SBF solution of glasses SG (A), SGCu(ox) (B) and SGCu(red) (C) as such and after soaking in SBF solution: (a) samples as-synthesized, (b, c, d and e), after 1,4,7 and 14 days of reaction, respectively.

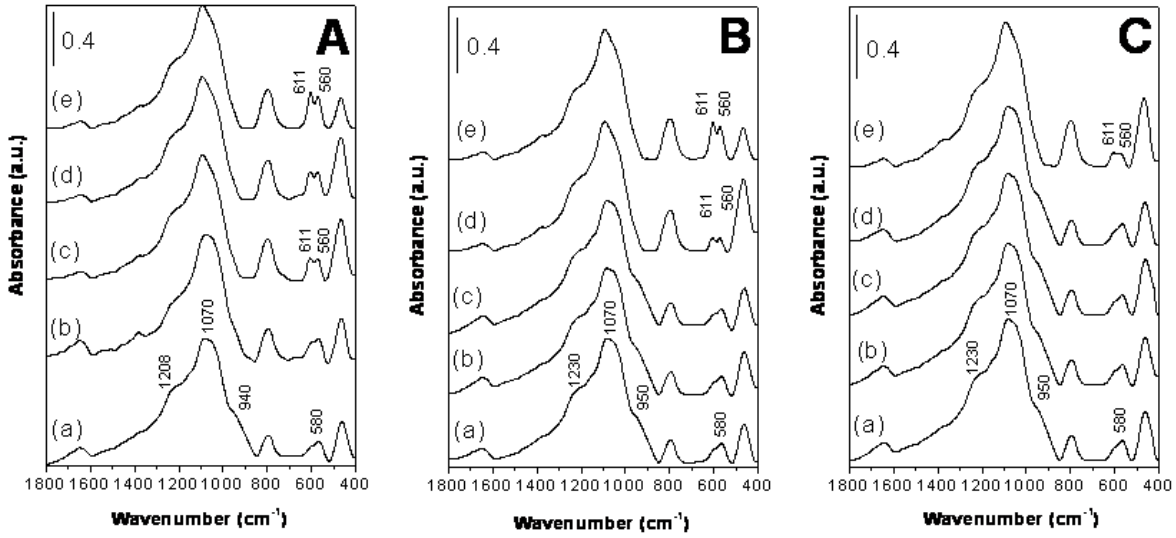

Figure 6. Absorbance differential IR spectra (in the region 2200-2080) relative to the adsorption of CO at 77K on SG (A), SGCu(ox) (B) and SGCu(red)-(C) after 14 days of reaction in SBF in contact with (a) 50 Torr of CO; (b) 25 Torr of CO; (c) 10 Torr of CO; (d) 5 Torr of CO; (e) 2 Torr of CO. Differential spectra were obtained with respect to the background spectrum of the glass outgassed at 423K (after a preliminary treatment at 673K and subsequent rehydration with purified distilled water at RT; see text).

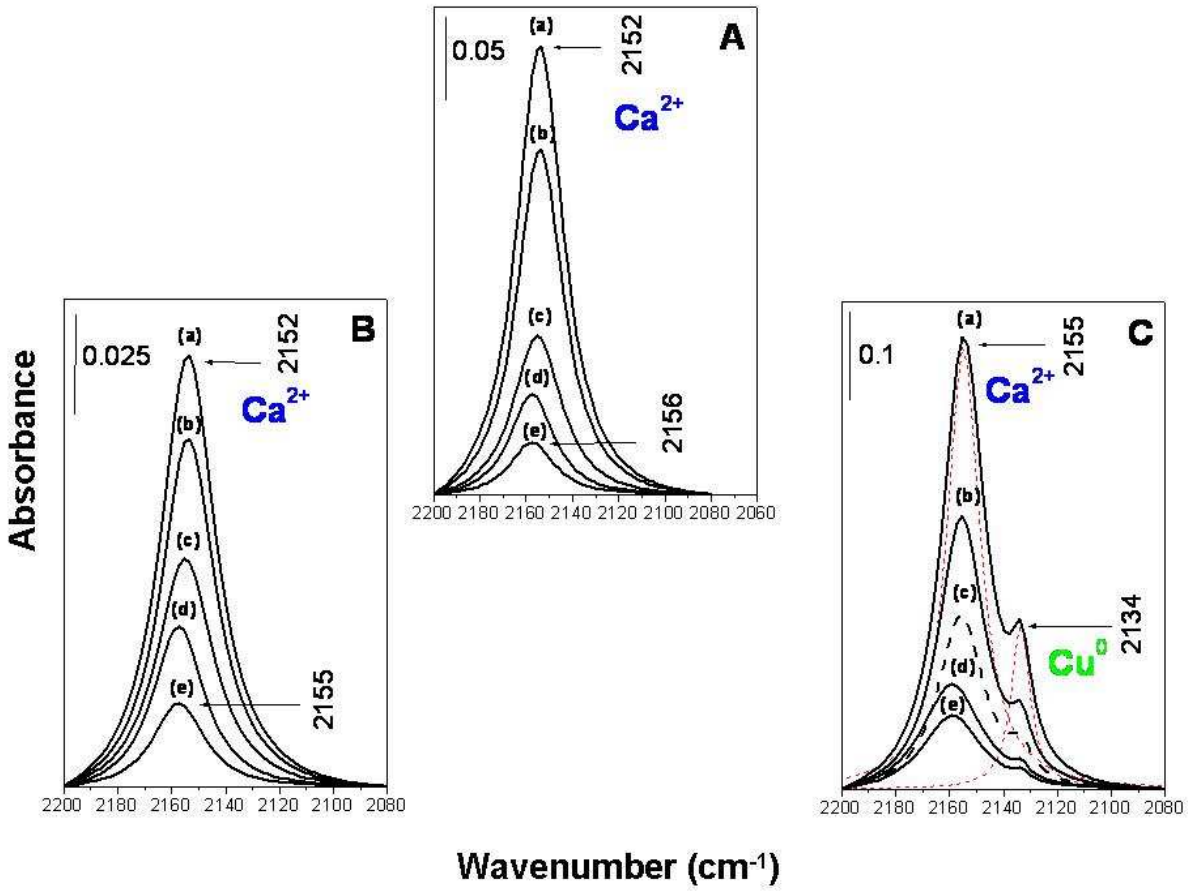

Figure 7. TEM image of centrifugate SBF solution after 7 days of SGCu(red) soaking.

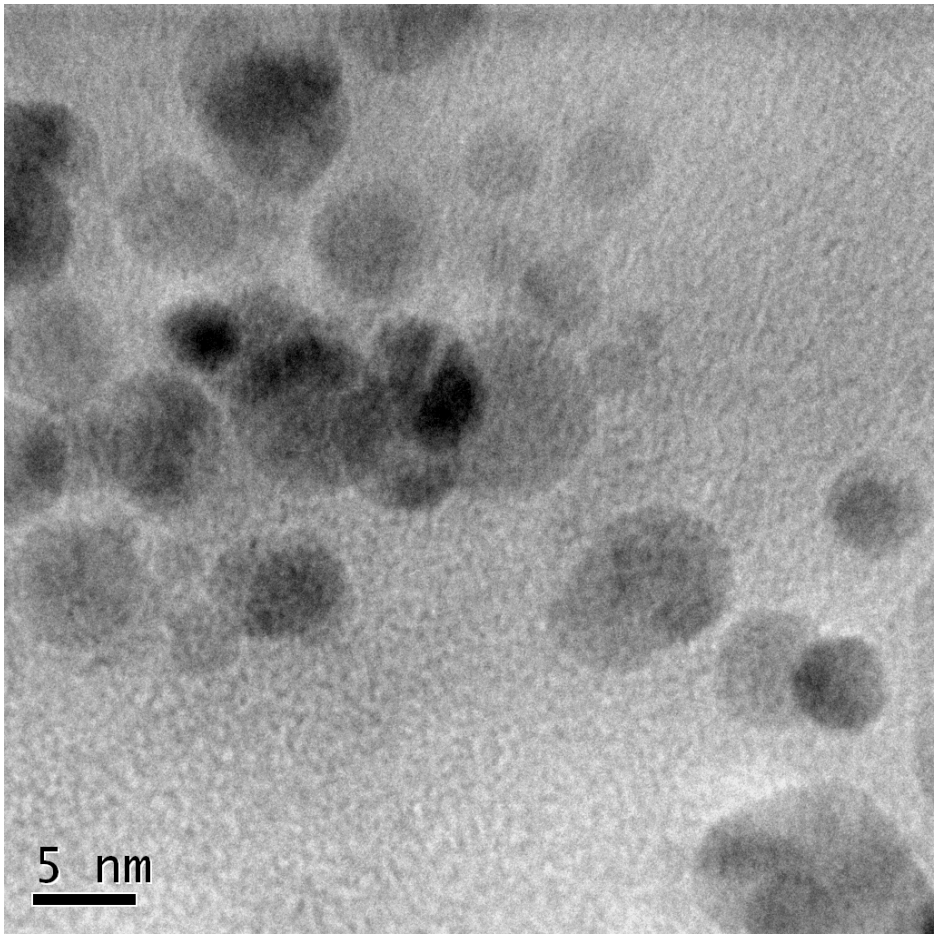

Tables

Table 1. Experimental composition in molar% of studied glasses

	SiO_2 [%mol]	CaO [%mol]	P_2O_5 [%mol]	CuO [%mol]
SG	79.7 ± 0.8	15.1 ± 0.5	5.2 ± 0.6	
SGCu(ox)	79.5 ± 1.0	14.6 ± 0.5	4.8 ± 0.3	1.1± 0.1
SGCu(red)	79.5 ± 1.2	13.0 ± 1.0	4.8 ± 0.3	2.9 ± 1.7

± std. dev. - the standard deviation was obtained by independent determinations on 4 different samples of same theoretical composition.

Table 2. N_2 adsorption data on the as-synthesized samples.

Samples	BET (N_2) (m^2/g)	t-plot micropore area (between 3.5 and 5 Å) (N_2) (m^2/g)	BJH pore area (between 17 and 3000 Å) (N_2) (m^2/g)	BJH adsorption average pore width (N_2) (Å)
SG	361	43	109	21
SGCu(ox)	298	23	140	26
SGCu(red)	137	85	12	21

Table 3. Concentration (ppm) of species. (± *std. dev.,* reported data are an average of four different determinations on the same sample solution)

	Time [Days]	***Si [ppm]***	***Ca [ppm]***	***P [ppm]***	***Cu [ppm]***
	SBF (t=0)	0	98*	30*	0
SG	*1*	58	296	165	
	4	56	290	155	
	7	58	285	150	
	14	62	275	140	
SGCu(ox)	*1*	38	181	103	1
	4	57	185	100	3
	7	70	187	108	5
	14	78	136	60	2
SGCu(red)	*1*	49	137	89	38
	4	68	145	104	48
	7	74	137	91	65
	14	75	144	82	53

* the theoretical concentration of Ca and P are 96 and 31 ppm, respectively
± *std. dev*. were lower then 4% for Si, Ca, P and Cu

References

1. Aina, V.; Ghigo, D.; Marchis, T.; Cerrato, G.; Laurenti, E.; Morterra, C.; Malavasi, G.; Lusvardi, G.; Menabue, L.; Bergandi, L. Novel bio-conjugate materials: soybean peroxidase immobilized on bioactive glasses containing Au nanoparticles. *Journal of Materials Chemistry* **2011,** 21, 10970-10981.
2. Hutten, A.; Sudfeld, D.; Ennen, I.; Reiss, G.; Hachmann, W.; Heinzmann, U.; Wojczykowski, K.; Jutzi, P.; Saikaly, W.; Thomas, G. New magnetic nanoparticles for biotechnology. *Journal of Biotechnology* **2004,** 112, 47-63.
3. Sondi, I.; Siiman, A.; Matijevic, E. Synthesis of CdSe nanoparticles in the presence of aminodextran as stabilizing and capping agent. *Journal of Colloid and Interface Science* **2004,** 275, 503-507.
4. Sondi, I.; Salopek-Sondi, B. Silver nanoparticles as antimicrobial agent: a case study on E-coli as a model for Gram-negative bacteria. *Journal of Colloid and Interface Science* **2004,** 275, 177-182.
5. Cao, H.; Liu, X. Silver nanoparticles-modified films versus biomedical device-associated infections. *Wiley Interdisciplinary Reviews-Nanomedicine and Nanobiotechnology* **2010,** 2, 670-684.
6. Lusvardi, G.; Malavasi, G.; Aina, V.; Bertinetti, L.; Cerrato, G.; Magnacca, G.; Morterra, C.; Menabue, L. Bioactive Glasses Containing Au Nanoparticles. Effect of Calcination Temperature on Structure, Morphology, and Surface Properties. *Langmuir* **2010,** 26, 10303-10314.
7. Jain, S.; Hirst, D. G.; O'Sullivan, J. M. Gold nanoparticles as novel agents for cancer therapy. *British Journal of Radiology* **2012,** 85, 101-113.
8. Parveen, S.; Misra, R.; Sahoo, S. K. Nanoparticles: a boon to drug delivery, therapeutics, diagnostics and imaging. *Nanomedicine-Nanotechnology Biology and Medicine* **2012,** 8, 147-166.
9. Zanoli, L. M.; D'Agata, R.; Spoto, G. Functionalized gold nanoparticles for ultrasensitive DNA detection. *Analytical and Bioanalytical Chemistry* **2012,** 402, 1759-1771.
10. Chase, P. A.; Gebbink, R.; van Koten, G. Where organometallics and dendrimers merge: the incorporation of organometallic species into dendritic molecules. *Journal of Organometallic Chemistry* **2004,** 689, 4016-4054.
11. Keng, P. Y.; Shim, I.; Korth, B. D.; Douglas, J. F.; Pyun, J. Synthes is and self-assembly of polymer-coated ferromagnetic nanoparticles. *Acs Nano* **2007,** 1, 279-292.
12. Wildgoose, G. G.; Banks, C. E.; Compton, R. G. Metal nanopartictes and related materials supported on carbon nanotubes: Methods and applications. *Small* **2006,** 2, 182-193.
13. Mohan, R.; Shanmugharaj, A. M.; Hun, R. S. An efficient growth of silver and copper nanoparticles on multiwalled carbon nanotube with enhanced antimicrobial activity. *Journal of Biomedical Materials Research Part B-Applied Biomaterials* **2011,** 96B, 119-126.
14. Valodkar, M.; Rathore, P. S.; Jadeja, R. N.; Thounaojam, M.; Devkar, R. V.; Thakore, S. Cytotoxicity evaluation and antimicrobial studies of starch capped water soluble copper nanoparticles. *Journal of Hazardous Materials* **2012,** 201, 244-249.
15. Simchi, A.; Tamjid, E.; Pishbin, F.; Boccaccini, A. R. Recent progress in inorganic and composite coatings with bactericidal capability for orthopaedic applications. *Nanomedicine-Nanotechnology Biology and Medicine* **2011,** 7, 22-39.
16. Luz, G. M.; Mano, J. F. Preparation and characterization of bioactive glass nanoparticles prepared by sol-gel for biomedical applications. *Nanotechnology* **2011,** 22, 49-55.
17. Zhang, N.; Gao, Y.; Zhang, H.; Feng, X.; Cai, H.; Liu, Y., Preparation and characterization of core-shell structure of SiO_2-Cu antibacterial agent. *Colloids and Surfaces B-Biointerfaces* **2010,** 81, 537-543.
18. Zhang, W.; Chu, P. K. Enhancement of antibacterial properties and biocompatibility of polyethylene by silver and copper plasma immersion ion implantation. *Surface and Coatings Technology* **2008,** 203, 909-912.
19. Caruso, F.; Spasova, M.; Saigueirino-Maceira, V.; Liz-Marzan, L. M. Multilayer assemblies of silica-encapsulated gold nanoparticles on decomposable colloid templates. *Advanced Materials* **2001,** 13, 1090-1096.

20. Akhavan, O.; Ghaderi, E. Cu and CuO nanoparticles immobilized by silica thin films as antibacterial materials and photocatalysts. *Surface and Coatings Technology* **2010,** 205, 219-223.
21. Kim, Y. H.; Lee, D. K.; Cha, H. G.; Kim, C. W.; Kang, Y. C.; Kang, Y. S., Preparation and characterization of the antibacterial Cu nanoparticle formed on the surface of SiO_2 nanoparticles. *Journal of Physical Chemistry B* **2006,** 110, 24923-24928.
22. Arvizo, R.R.; Bhattacharyya, S.; Kudgus, R. A.; Giri, K.; Bhattacharya, R.; Mukherjee, P. Intrinsic therapeutic applications of noble metal nanoparticles: past, present and future. *Chemical Society Reviews* **2012,** 41, 2943-2970.
23. Pan, Y.; Du, X.; Zhao, F.; Xu, B. Magnetic nanoparticles for the manipulation of proteins and cells. *Chemical Society Reviews* **2012,** 41, 2912-2942.
24. Sailor, M. J.; Park, J.-H., Hybrid Nanoparticles for Detection and Treatment of Cancer. *Advanced Materials* **2012,** 24, 3779-3802.
25. Li, R.; Clark, A.E.; Hench, L.L. An Investigation of bioactive glass powders by sol-gel processing. *Journal of Applied Biomaterials* **1991,** 2, 231-239.
26. Xynos, I. D.; Edgar, A. J.; Buttery, L. D. K.; Hench, L. L.; Polak, J. M. Gene-expression profiling of human osteoblasts following treatment with the ionic products of Bioglass 45S5 dissolution. *Journal of Biomedical Materials Research* **2001,** 55, 151-157.
27. Xynos, I. D.; Edgar, A. J.; Ramachandran, M.; Buttery, L. D. K.; Hench, L. L.; Polak, J. M. Biochemical characterisation and gene expression profiling of human trabecular bone derived osteoblasts. *Journal of Pathology* **2001,** 193, 31A-31A.
28. Hoppe, A.; Gueldal, N. S.; Boccaccini, A. R., A review of the biological response to ionic dissolution products from bioactive glasses and glass-ceramics. *Biomaterials* **2011,** 32, 2757-2774.
29. Nedelec, J. M.; Courtheoux, L.; Jallot, E.; Kinowski, C.; Lao, J.; Laquerriere, P.; Mansuy, C.; Renaudin, G.; Turrell, S. Materials doping through sol-gel chemistry: a little something can make a big difference. *Journal of Sol-Gel Science and Technology* **2008,** 46, 259-271.
30. Bonici, A.; Lusvardi, G.; Malavasi, G.; Menabue, L.; Piva, A. Synthesis and characterization of bioactive glasses functionalized with Cu nanoparticles and organic molecules. *Journal of the European Ceramic Society* **2012,** 32, 2777-2783.
31. Brunauer, S.; Emmet, P. H.; Teller, E. J., *J. Am. Chem. Soc.* **1938,** 60, 309-320.
32. Barrett, E. P.; Joyner, L. S.; Halenda, P. P. *J.Am.Chem.Soc.* **1951,** 73, 373-778.
33. Lippens, B. C.; de Boer, J. H., *J. Catal.* **1965,** 4, 319-331.
34. Gregg, S. J.; Sing, K. S. W., *Adsorption, Surface Area and Porosity*: 2nd Edition. Academic Press. San Diego,CA. 1995.
35. Hair, M. L., *Infrared Spectroscopy in Surface Science,* . Dekker: New York,1967.
36. Little, L. H., *Infrared Spectra of Adsorbed Species* Academic Press: New York, 1966.
37. Marchese, L.; Bordiga, S.; Coluccia, S.; Martra, G.; Zecchina, A. Strucure of the surface sites of delta-Al_2O_3 as determined by high-resolution transmission microscopy, computer modelling and infrared-spectroscopy of adsorbed CO. *Journal of the Chemical Society-Faraday Transactions* **1993,** 89, 3483-3489.
38. Morterra, C.; Cerrato, G.; Di Ciero, S. IR study of the low temperature adsorption of CO on tetragonal zirconia and sulfated tetragonal zirconia. *Applied Surface Science* **1998,** 126, 107-128.
39. Morterra, C.; Magnacca, G.; Bolis, V.; Cerrato, G.; Baricco, M.; Giachello, A.; Fucale, M. Structural, morphological and surface chemical features of Al_2O_3 catalyst supports stabilized with CeO_2. In *Catalysis and Automotive Pollution Control*, **1995,** 96,361-373.
40. Kokubo, T.; Takadama, H. How useful is SBF in predicting in vivo bone bioactivity? *Biomaterials* **2006,** 27, 2907-2915.
41. Aina, V.; Morterra, C.; Lusvardi, G.; Malavasi, G.; Menabue, L.; Shruti, S.; Bianchi, C.L.; Bolis V., Bolis, V. Ga-Modified (Si-Ca-P) Sol-Gel Glasses: Possible Relationships between Surface Chemical Properties and Bioactivity. *J. of Phys. Chem. C,* **2011**, 115, 22461-22474.
42. Malavasi, G.; Ferrari, E.; Lusvardi, G.; Aina, V.; Fantini, F.; Morterra, C.; Pignedoli, F.; saladini, M.; Menabue, L.,The role of coordination chemistry in the development of innovative gallium-based bioceramics: the case of curcumin. *J. of Mat. Chem.*, **2011**, 21, 5027-5037.

43. Foster, A. J.; Lobo, R. F. Identifying reaction intermediates and catalytic active sites through in situ characterization techniques. *Chemical Society Reviews* **2010,** 39, 4783-4793.
44. Lamberti, C.; Zecchina, A.; Groppo, E.; Bordiga, S., Probing the surfaces of heterogeneous catalysts by in situ IR spectroscopy. *Chemical Society Reviews* **2010,** 39, 4951-5001.
43. Morterra, C.; Cerrato, G.; Bolis, V.; DiCiero, S.; Signoretto, M. On the strength of Lewis- and Bronsted-acid sites at the surface of sulfated zirconia catalysts. *Journal of the Chemical Society-Faraday Transactions* **1997,** 93, 1179-1184.
45. Byeon, J. H.; Yoon, K. Y.; Park, J. H.; Hwang, J. Characteristics of electroless copper-depo sited activated carbon fibers for antibacterial action and adsorption-desorption of volatile organic compounds. *Carbon* **2007,** 45, 2313-2316.
47. Shruti, S.; Salinas, A. J.; Malavasi, G.; Lusvardi, G.; Menabue, L.; Ferrara, C.; Mustarelli, P.; Vallet-Regi, M. Structural and in vitro study of cerium, gallium and zinc containing sol-gel bioactive glasses. *Journal of Materials Chemistry* **2012,** 22, 13698-13706.